Optical microdisk cavities with rough sidewalls: A perturbative approach based on weak boundary deformations

Jan Wiersig* and Julius Kullig
Institut für Theoretische Physik, Otto-von-Guericke-Universität Magdeburg, Postfach 4120, D-39016 Magdeburg, Germany
(Received 13 March 2017; published 4 May 2017)

A recently developed perturbation theory for microdisk cavities with weak boundary deformation is applied to the problem of surface roughness. Explicit and transparent formulas for the variance of the frequency splitting and the expectation values of the decay rates are derived for transverse magnetic polarization. For a Gaussian correlation function we demonstrate excellent agreement of our statistical theory with full numerical simulations. The numerical simulations also reveal the chirality of mode pairs in rough microdisks.

DOI: 10.1103/PhysRevA.95.053815

I. INTRODUCTION

The study of optical microcavities has been an important interdisciplinary topic in fundamental and applied research [1–4]. One reason is that microcavities can trap light for a long time τ in a very small volume. This ability is often limited by surface roughness [5–10]. The effect of surface roughness depends strongly on the fabrication process, the material system, and the geometry. We restrict ourselves to microdisk cavities [11–13], which confine light by total internal reflection at the circular-shaped dielectric boundary. Surface roughness at the sidewalls of such cavities has been studied experimentally [7,8,10], numerically [14–16], and theoretically using the volume element method [7,8,10,17].

Usually surface roughness is considered an undesirable property, but sometimes it can be beneficial. For example, it has been demonstrated that microdisk lasers can be controlled by local refractive index perturbations and spatially nonuniform pumping provided that surface roughness has already broken the rotational symmetry [18–20]. Another interesting example is the study of dynamical localization in microdisks with strong surface roughness [21–25].

Microdisks with a smooth boundary deformation have been intensively studied for directional light emission [26–28] and as model systems for wave chaos [4,29]. For weak boundary deformations a perturbation theory has been developed which allows one to compute the quality factor $Q = \omega\tau$, the resonant frequency ω, and the near- and far-field patterns of the modes. Originally, the perturbation theory was restricted to a deformed boundary with a mirror-reflection symmetry [30,31]. This restriction avoids having to deal with the degeneracy of the mode pairs in the unperturbed disk. This nondegenerate perturbation theory has been applied successfully to a variety of different geometries [31–37]. The degenerate perturbation theory for the generic case of a deformed boundary without any mirror-reflection symmetry has been introduced only recently [38].

The aim of the present paper is to apply the degenerate perturbation theory for weak boundary deformations to the problem of surface roughness. It is shown that this approach leads to analytical formulas that allow one to easily calculate the variance of the frequency splitting and the expected decay rates. In contrast to previous approaches based on the volume element method [7,8,10,17,39,40], the present derivation is transparent and rather general.

This paper is organized as follows. Section II introduces the mode equation for deformed and circular microcavities. In Sec. III we review the relevant results of the degenerate perturbation theory. Section IV deals with general aspects of surface roughness in microdisks. Section V derives the perturbative expressions for the rough disk. The obtained formulas are compared to numerical calculations in Sec. VI and to experimental data from the literature in Sec. VII. Finally, we conclude in Sec. VIII.

II. MODE EQUATION FOR DEFORMED AND CIRCULAR MICROCAVITIES

Within the effective index approximation, Maxwell's equations reduce to a two-dimensional scalar mode equation [41],

$$-\nabla^2\psi = n^2(x,y)\frac{\omega^2}{c^2}\psi, \tag{1}$$

with the speed of light in vacuum, c, and the effective index of refraction $n(x,y)$ which is assumed to be $n > 1$ inside the cavity and $n = 1$ outside. In the effective index approximation the two polarizations of the light are decoupled into transverse magnetic (TM) and transverse electric (TE) polarization. TM polarized light has the electric field vector $\vec{E}(x,y,t) \propto (0,0,\mathrm{Re}[\psi(x,y)e^{-i\omega t}])$ perpendicular to the cavity plane. The wave function ψ and its normal derivative $\partial_\nu\psi$ are continuous across the cavity boundary. In the case of TE polarization, ψ represents the z component of the magnetic field vector H_z, with ψ and $n(x,y)^{-2}\partial_\nu\psi$ being continuous across the boundary [41]. With Sommerfeld's outgoing-wave condition the solutions of the mode equation (1) are quasibound states with decay rate $1/\tau = -2\,\mathrm{Im}\,\omega > 0$. The quality factor of the given mode is $Q = -\mathrm{Re}\,\omega/(2\,\mathrm{Im}\,\omega)$.

For the special case of a circular cavity with radius R the mode equation (1) including the boundary conditions can be solved analytically in polar coordinates (r,ϕ) with the ansatz

$$\psi(r,\phi) = \begin{cases} \frac{J_m(nkr)}{J_m(nx)}e^{im\phi} & \text{for } r \leqslant R \\ \frac{H_m(kr)}{H_m(x)}e^{im\phi} & \text{for } r > R. \end{cases} \tag{2}$$

Here, $m \in \mathbb{Z}$ is the azimuthal mode number, and J_m and H_m are the Bessel and Hankel functions of the first kind and

*Corresponding author: jan.wiersig@ovgu.de

order m. For TM polarization with fixed m, the complex (dimensionless) frequencies $x = kR = \omega R/c$ are given by the roots of

$$S_m(x) = n\frac{J_m'}{J_m}(nx) - \frac{H_m'}{H_m}(x) \tag{3}$$

and are labeled by the radial mode number $l \in \mathbb{N}_+$. Here, a prime denotes the first derivative with respect to the argument of the function. Note that such determined frequencies x depend only on l and $|m|$; i.e., the frequencies are twofold degenerate for $m \neq 0$.

III. ESSENTIALS OF THE PERTURBATION THEORY

The degenerate perturbation theory in Ref. [38] treats a boundary deformation of the type

$$r(\phi) = R + \lambda f(\phi) \tag{4}$$

with formal perturbation parameter λ and 2π-periodic deformation function $f(\phi)$ such that $|\lambda f(\phi)| \ll R$. As in Ref. [30], the theory is restricted to TM polarization but the deformation function is not required to be symmetric. The wave function of the deformed cavity is expanded in the solutions of the circular disk [Eq. (2)].

For a chosen pair of mode numbers (m,l) the order $O(\lambda^0)$ gives the frequency x_0 of the circular cavity. For the frequency of the perturbed mode $x = kR$ it is found up to order $O(\lambda^2)$,

$$x^{(\mu)} = x_0 + \lambda x_1^{(\mu)} + \lambda^2 x_2^{(\mu)}, \tag{5}$$

with mode index $\mu \in \{0,1\}$ labeling the modes in the given pair. The first-order correction is given by

$$x_1^{(\mu)} = -x_0(A_0 + e^{-2iz_0}A_{-2m}) \tag{6}$$

with

$$z_0 = -\frac{1}{4}\mathrm{Arg}\left(\frac{A_{2m}}{A_{-2m}}\right) + \mu\frac{\pi}{2} \tag{7}$$

and dimensionless Fourier coefficients of $f(\phi)$,

$$A_q = \frac{1}{2\pi R}\int_0^{2\pi} f(\phi)e^{iq\phi}\,d\phi. \tag{8}$$

The obvious relation $A_{-q} = A_q^*$ holds since $f(\phi)$ is a real-valued function. Equation (6) can be rewritten as

$$x_1^{(\mu)} = -x_0(A_0 \pm |A_{2m}|), \tag{9}$$

where $+$ $(-)$ refers to the $\mu = 0$ ($\mu = 1$) mode.

The second-order correction is written in a more compact form than in Ref. [38]:

$$\begin{aligned} x_2^{(\mu)} = x_0\Bigg\{ & \frac{3}{2}\left(\frac{x_1^{(\mu)}}{x_0}\right)^2 - \frac{1}{2}(B_0 + e^{-2iz_0}B_{-2m}) + x_0\frac{H_m'}{H_m}(x_0)\left[\left(\frac{x_1^{(\mu)}}{x_0}\right)^2 - (B_0 + e^{-2iz_0}B_{-2m})\right] \\ & - \frac{1}{2}(n^2-1)x_0\sum_{p\neq\pm m}\frac{1}{S_p(x_0)}[|A_{m-p}|^2 + |A_{p+m}|^2 + e^{-2iz_0}A_{-m-p}A_{p-m} + e^{2iz_0}A_{m-p}A_{p+m}] \\ & - \frac{1}{4}\left[1 + 2x_0\frac{H_m'}{H_m}(x_0)\right](e^{2iz_0}B_{2m} - e^{-2iz_0}B_{-2m})\Bigg\} \end{aligned} \tag{10}$$

with dimensionless Fourier coefficients of $f^2(\phi)$,

$$B_q = \frac{1}{2\pi R^2}\int_0^{2\pi} f^2(\phi)e^{iq\phi}\,d\phi \tag{11}$$

$$= \sum_{j=-\infty}^{\infty} A_j A_{j-q}^*. \tag{12}$$

Also here $B_{-q} = B_q^*$ holds since $f(\phi)$ is real valued.

IV. SURFACE ROUGHNESS: GENERAL ASPECTS

The study of wave scattering at rough surfaces has a long history (see, e.g., Ref. [42]). In the case of microdisks it has been observed that the etch process results in residual surface roughness often with uniform corrugations along the vertical direction (see, e.g., Refs. [43–45]). This justifies the effective index approximation used in our theory.

The rough boundary of a microdisk of radius R is usually described [10,16] by

$$r(\phi) = R + \xi(\phi), \tag{13}$$

where $\xi(\phi) = \xi(\phi + 2\pi)$ is a real random variable. A so-called wide-sense stationary random process [46] is assumed; i.e., for all values of the angles ϕ and ϕ',

$$\langle \xi(\phi)\rangle = 0, \tag{14}$$

$$\langle [\xi(\phi)]^2\rangle = \sigma^2, \tag{15}$$

and

$$\langle \xi(\phi)\xi(\phi')\rangle = \sigma^2\mathcal{W}(\phi - \phi'). \tag{16}$$

Here and below, the angular bracket $\langle\cdots\rangle$ stands for an ensemble average over all realizations of the random process. This procedure has to be distinguished from a spatial average over the angle ϕ of a fixed realization. Only for extended systems such as an infinite waveguide [42] are both types of the average assumed to be equivalent (ergodicity). The positive quantity σ is called the roughness standard deviation. $\mathcal{W}(\phi) \in \mathbb{R}$ is the azimuthal correlation function which is a 2π-periodic function of ϕ due to the 2π periodicity of $\xi(\phi)$. Consistent with Eq. (15), $\mathcal{W}(0) = 1$ is chosen. Moreover,

from definition (16) it follows that [46] (i) $\mathcal{W}(-\phi) = \mathcal{W}(\phi)$, (ii) $|\mathcal{W}(\phi)| \leqslant \mathcal{W}(0)$, and (iii) the Fourier transform

$$W_q = \frac{1}{2\pi}\int_0^{2\pi} \mathcal{W}(\phi) e^{iq\phi}\, d\phi \tag{17}$$

is real and non-negative. W_q is also named the roughness power spectrum.

By direct measurements of the surface profile of silicon microdisk sidewalls [8] it has been demonstrated that the correlation function $\mathcal{W}$ is well approximated by a Gaussian

$$\mathcal{W}(\phi - \phi') = e^{-(\phi-\phi')^2/\Theta_c^2} \tag{18}$$

with correlation angle $\Theta_c > 0$. Equivalently, one can use the correlation length $L_c = R\Theta_c$. It should be pointed out that the correlation function in Eq. (18) lacks a proper 2π periodicity, so this equation only makes sense for $\Theta_c \ll 2\pi$. For general Θ_c we modify the equation to

$$\mathcal{W}(\phi - \phi') = \frac{1}{\vartheta(\Theta_c)} \sum_{j=-\infty}^{\infty} e^{-(\phi-\phi'+2\pi j)^2/\Theta_c^2}, \tag{19}$$

where $\vartheta(\Theta_c) = \sum_{j=-\infty}^{\infty} e^{-(2\pi j)^2/\Theta_c^2}$ ensures that $\mathcal{W}(0) = 1$. $\vartheta(\Theta_c)$ can also be expressed by $\vartheta(\Theta_c) = \vartheta_3(0, e^{-4\pi^2/\Theta_c^2})$, where ϑ_3 is one of the Jacobi theta functions [47]. The modification (19) takes care of the fact that ξ at $\phi = \varepsilon$ and $\phi' = 2\pi - \varepsilon$ for $0 < \varepsilon \ll \Theta_c$ are strongly correlated, which would be ignored by Eq. (18). For realistic Θ_c, Eqs. (18) and (19) give nearly identical results. For instance, for the maximal value of Θ_c used in this work, 0.2, the value of $\vartheta(\Theta_c)$ is extremely close to 1: $|\vartheta(\Theta_c) - 1| \approx 10^{-427}$. Hence, also Eq. (19) is fully consistent with the experiments in Ref. [8].

V. SURFACE ROUGHNESS: PERTURBATION THEORY

The same structure of Eqs. (4) and (13) suggests that for $\sigma \ll R$ the perturbation theory for weak boundary deformations can be applied to rough microdisks simply by using $\lambda f(\phi) = \xi(\phi)$ and performing an appropriate ensemble average.

First let us note that Eqs. (14)–(17) imply that the Fourier coefficients of the deformation function, A_q, can be considered as independent random variables with

$$\langle A_q \rangle = 0, \tag{20}$$

$$\langle A_q A_p^* \rangle = \frac{\sigma^2}{R^2} W_q\, \delta_{q,p}, \tag{21}$$

where $\delta_{q,p}$ is the Kronecker delta. For the special case of the Gaussian correlation function we get for the roughness power spectrum

$$W_q = \frac{1}{2\sqrt{\pi}} \frac{\Theta_c}{\vartheta(\Theta_c)} e^{-q^2 \frac{\Theta_c^2}{4}}. \tag{22}$$

This expression is valid also for general Θ_c as long as Eq. (19) is used.

A. Frequency splitting

The first quantity that we consider is the (real) frequency splitting,

$$\Delta x = \mathrm{Re}(x^{(0)} - x^{(1)}). \tag{23}$$

Its expectation value vanishes, $\langle \Delta x \rangle = 0$, since both modes are equivalent. At first glance this seems to be in contradiction with Eq. (9). However, in the perturbation theory the two modes of a given pair are no longer equivalent since the mode with $\mu = 0$ is the selected one with smaller $\mathrm{Re}(x_1^{(\mu)})$. In other words, when we do numerical simulations or experiments we cannot decide which of the modes is the one with frequency $x^{(0)}$ and which is the one with $x^{(1)}$. Of course, one could alternatively consider $\langle |\Delta x| \rangle$ as a proper measure for the expected frequency splitting. However, in our statistical theory it is more natural to look at the variance of the frequency splitting from the zero mean:

$$\mathrm{Var}(\Delta x) = \langle (\Delta x)^2 \rangle. \tag{24}$$

Plugging in the first-order result of the perturbation theory for $x^{(\mu)}$ in Eq. (9) and taking advantage of Eq. (21) gives straightforwardly the first central result,

$$\mathrm{Var}(\Delta x) = 4\,\mathrm{Re}(x_0)^2 \frac{\sigma^2}{R^2} W_{2m}. \tag{25}$$

The frequency splitting is determined by the coupling of the modes m and $-m$, with strength proportional to $W_{m-(-m)} = W_{2m}$. For the frequency splitting we restrict ourselves to the first-order perturbation theory. Second-order contributions would require higher-order moments which are not provided by Eqs. (20) and (21).

For the special case of the Gaussian correlation function we get with Eq. (22)

$$\mathrm{Var}(\Delta x) = \frac{2}{\sqrt{\pi}} \mathrm{Re}(x_0)^2 \frac{\sigma^2}{R^2} \frac{\Theta_c}{\vartheta(\Theta_c)} e^{-m^2\Theta_c^2}. \tag{26}$$

Ignoring the weak dependence of $\vartheta(\Theta_c)$ on the correlation angle Θ_c in the relevant regime, it can be seen that $\mathrm{Var}(\Delta x)$ as a function of Θ_c has a global maximum at $\Theta_c = 1/(\sqrt{2}m)$.

B. Decay rates

For computing the expectation value of the decay rate for mode μ,

$$\gamma^{(\mu)} = -\langle \mathrm{Im}(x^{(\mu)}) \rangle, \tag{27}$$

we simplify the terms from the first- and second-order contributions by restricting ourselves to well-confined modes, i.e., $\gamma_0 = |\mathrm{Im}(x_0)| \ll \mathrm{Re}(x_0)$, and highly excited states, i.e., $\mathrm{Re}(x_0) \gg 1$, which covers all cases of practical interest. The first assumption immediately implies that the first-order contribution [Eq. (9)] to $\gamma^{(\mu)}$ is zero as x_0 is replaced by $\mathrm{Re}(x_0)$ for well-confined modes. To determine the second-order contributions, we first derive from Eq. (11)

$$\langle B_q \rangle = \frac{\sigma^2}{R^2}\, \delta_{q,0}. \tag{28}$$

Second, with $A_q = |A_q| e^{i\varphi_q}$, $\varphi_q \in \mathbb{R}$, and Eqs. (7) and (12) we write

$$\langle e^{-2iz_0} B_{-2m} \rangle = e^{-i\mu\pi} \sum_j \langle |A_j||A_{j+2m}| e^{i(\varphi_{2m} + \varphi_j - \varphi_{j+2m})} \rangle. \tag{29}$$

Since the A_q are independent random variables, so are the angles φ_q. We conclude

$$\langle e^{-2iz_0} B_{-2m} \rangle = 0 = \langle e^{2iz_0} B_{2m} \rangle. \tag{30}$$

The same kind of reasoning gives

$$\langle e^{-2iz_0} A_{-m-p} A_{p-m}\rangle = 0 = \langle e^{2iz_0} A_{m-p} A_{p+m}\rangle. \tag{31}$$

Third, we conclude from Eq. (9) that $x_1^{(\mu)}/x_0$ is real. Fourth, for highly excited states which are well confined [$m > \mathrm{Re}(x_0)$] the quotient $H_m'(x_0)/H_m(x_0)$ is real [30]. Putting everything together, we see that from Eqs. (5), (9), and (10) only the following contributions remain:

$$\gamma^{(\mu)} = \gamma_0 + \frac{(n^2-1)\mathrm{Re}(x_0)^2\sigma^2}{2R^2}\,\mathrm{Im}\sum_{p\neq\pm m}\frac{W_{m-p}+W_{p+m}}{S_p(x_0)}. \tag{32}$$

Using the fact that the right-hand side of this equation does not depend on the mode index μ, the equality $S_{-p} = S_p$, and the definition of the real-valued quantity

$$D_p(x) = \frac{n^2-1}{\pi}\mathrm{Im}\,\frac{1}{S_p(x)}, \tag{33}$$

we can write as the second central result

$$\gamma = \gamma_0 + \pi\,\mathrm{Re}(x_0)^2\frac{\sigma^2}{R^2}\sum_{p\neq\pm m} W_{m-p} D_p(x_0). \tag{34}$$

In contrast to the frequency splitting, which results from a coupling of the modes m and $-m$ within the degenerate mode pair, the decay induced by the surface roughness is determined by the coupling to other modes $p \neq \pm m$ with strength proportional to $W_{m-p}D_p(x_0)$. To interpret the weight $D_p(x_0)$ we note the relation for real-valued x [48],

$$d(x) - d^{(0)}(x) = \frac{n^2-1}{\pi}\sum_{p=-\infty}^{\infty}\mathrm{Im}\,\frac{1}{S_p(x)} = \sum_{p=-\infty}^{\infty} D_p(x), \tag{35}$$

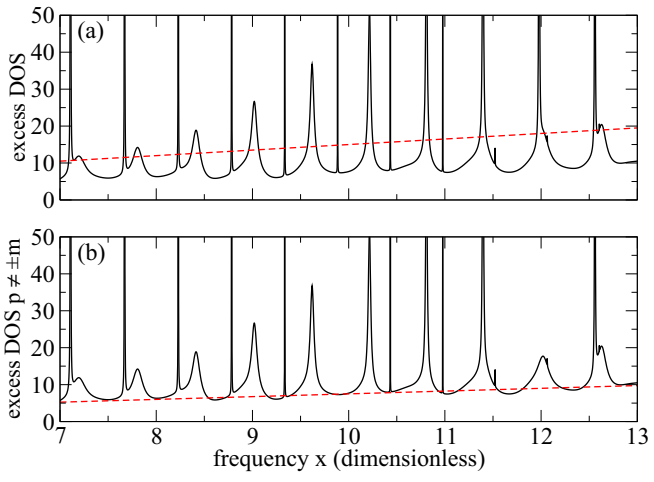

FIG. 1. (a) Excess DOS [Eq. (35)] (solid black curve) and its smooth part [Eq. (47)] (dashed red line) of the circular microdisk as a function of the dimensionless frequency x on the real axis. The refractive index is set to $n = 2$. (b) The solid black curve shows the right-hand side of Eq. (35) with the summands corresponding to $p = \pm m$ excluded. The dashed red line is the smooth part of the DOS divided by n.

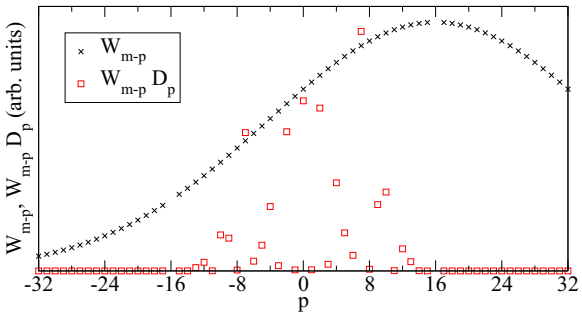

FIG. 2. Summands in Eq. (34) for a mode pair $(m,l) = (16,1)$ with refractive index $n = 2$. The correlation function is a Gaussian [Eq. (19)] with roughness standard deviation $\sigma/R = 0.005$ and correlation angle $\Theta_c = 0.07$. The summands with $p = \pm m$ are not shown since they do not appear in the sum [Eq. (34)].

where $d(x)$ is the optical density of states (DOS) in the presence of the circular microcavity; $d^{(0)}(x)$ is the DOS in the absence of the circular microcavity. The excess DOS $d(x) - d^{(0)}(x)$ is shown in Fig. 1(a). Hence, for $|\mathrm{Im}(x_0)| \ll \mathrm{Re}(x_0)$ we can interpret $D_p(x_0)$ as p-resolved excess DOS at frequency x_0.

For the Gaussian correlation function with Eq. (22) the explicit formula follows:

$$\gamma = \gamma_0 + \frac{(n^2-1)\mathrm{Re}(x_0)^2\sigma^2\Theta_c}{2\sqrt{\pi}R^2\vartheta(\Theta_c)}\sum_{p\neq\pm m}\mathrm{Im}\,\frac{e^{-(m-p)^2\frac{\Theta_c^2}{4}}}{S_p(x_0)}. \tag{36}$$

Figure 2 shows an example of the summands in Eq. (34) for the Gaussian correlation function [see also Eq. (36)]. It can be seen that only components with $|p| < m$ can contribute to the decay rate. The reason for this is twofold. First, the p-resolved excess DOS is for each radial mode number l approximately a Lorentzian with a linewidth that increases with decreasing $|p|$. This reflects the fact that the lifetime of modes in the circular cavity reduces with decreasing $|p|$. In particular, states with $|p| < \mathrm{Re}(x_0) \approx 10$ are not confined by total internal reflection [30]. Obviously, a broader peak has a better chance to significantly overlap with $x = \mathrm{Re}(x_0)$. This can be clearly seen in Fig. 3. Second, the frequency of a mode of the circular cavity increases with $|p|$. This implies

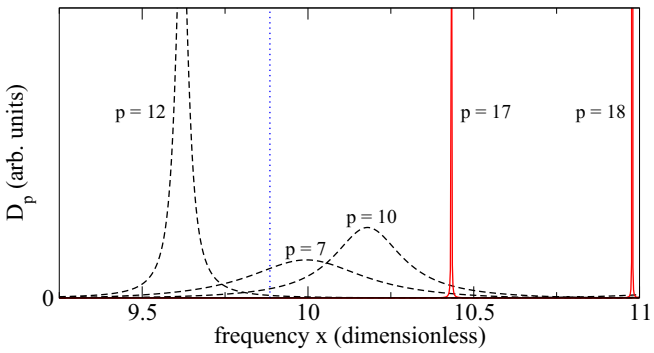

FIG. 3. The p-resolved excess DOS D_p [Eq. (33)] vs dimensionless frequency x for $n = 2$ and various p. D_p for $|p| > 16$ ($|p| < 16$) is shown as solid (dashed) curves. The dotted vertical line marks the value $x = \mathrm{Re}(x_0) \approx 9.8853$ for the mode pair $(m,l) = (16,1)$.

that for the same l the frequency belonging to a contribution with $|p| > m$ is already distant from the frequency of mode m. That is different for contributions with $|p| < m$ since the radial mode number l can be increased to come closer to the mode with azimuthal mode number m. For example, the peak with $p = 7$ in Fig. 3 corresponds to a radial mode number of $l = 4$, the peak with $p = 10$ corresponds to $l = 3$, and the peak with $p = 12$ corresponds to $l = 2$.

C. Applicability of the perturbation series

In this section we derive a condition for the validity of our theory. To do so, we remark that in the perturbation theory of Ref. [38] the first-order correction to the internal wave function is given by the coefficient

$$a_p = \frac{(n^2-1)x_0}{S_p(x_0)}(e^{iz_0}A_{m-p} + e^{-iz_0}A_{-m-p}) \tag{37}$$

for the contribution from mode $p \neq \pm m$ of the circular cavity. Assuming again $|\mathrm{Im}(x_0)| \ll \mathrm{Re}(x_0)$ it follows with the help of Eqs. (21) and (31) that

$$\langle |a_p|^2 \rangle = \frac{(n^2-1)^2 \mathrm{Re}(x_0)^2}{|S_p(x_0)|^2}\frac{\sigma^2}{R^2}(W_{m-p} + W_{p+m}). \tag{38}$$

We have to require a weak correction, i.e.,

$$\sqrt{\langle |a_p|^2 \rangle} \ll 1 \tag{39}$$

for each $p \neq \pm m$. For $1/|S_p|$ the following estimate is known [30]:

$$\frac{1}{|S_p(x)|} \sim \frac{n^2}{4}\frac{s_n}{n^2-1}x \tag{40}$$

with

$$s_n = 1 - \frac{2}{\pi}\left(\arcsin\frac{1}{n} + \frac{1}{n}\sqrt{1-\frac{1}{n^2}}\right). \tag{41}$$

For instance, $s_2 \approx 0.391$. Inserting Eq. (40) into Eq. (39) gives the condition

$$\frac{n^2}{4}s_n \mathrm{Re}(x_0)^2 \frac{\sigma}{R}\sqrt{W_{m-p} + W_{p+m}} \ll 1 \tag{42}$$

for each $p \neq \pm m$.

For the Gaussian correlation function with Fourier transform (22) we estimate with $e^{-(m-p)^2\Theta_c^2/4} < 1$ for $p \neq \pm m$ and $\vartheta(\Theta_c) \approx 1$

$$\frac{n^2}{4\pi^{1/4}}s_n \mathrm{Re}(x_0)^2 \frac{\sigma}{R}\sqrt{\Theta_c} \ll 1. \tag{43}$$

D. The smooth part of the excess DOS

In this section we simplify our result [Eq. (34)] by assuming that the Fourier transform W_{m-p} is a smooth and slowly varying function of p in the relevant regime $|p| \leqslant \mathrm{Re}(x_0)$. We expand W_{m-p} at $p = 0$ up to second order in p,

$$W_{m-p} \approx W_m - W_m' p + \tfrac{1}{2}W_m'' p^2. \tag{44}$$

The second-order term can be ignored for all relevant p provided that

$$\frac{W_m'' \mathrm{Re}(x_0)^2}{2W_m} \ll 1. \tag{45}$$

Plugging Eq. (44) into Eq. (34) we see that the first-order term drops out because p/S_p is an odd function of p, yielding

$$\gamma = \gamma_0 + \pi\,\mathrm{Re}(x_0)^2\frac{\sigma^2}{R^2}W_m \sum_{p\neq\pm m} D_p(x_0). \tag{46}$$

The sum is almost equal to the sum in the excess DOS (35). It is therefore tempting to use the excess DOS and replace it by its smooth part given by Weyl law [48] for real x,

$$\bar{d}(x) - \bar{d}^{(0)}(x) = \frac{n^2-1}{2}x. \tag{47}$$

This approximation correctly describes the mean behavior of the excess DOS, but it cannot account for the fluctuations which can be rather large [cf. Fig. 1(a)]. Moreover, there is a subtle difference between the two sums in Eqs. (46) and (35). In Eq. (46) the terms with $p = \pm m$ do not appear. Figure 1(b) shows that this corresponds to missing peaks in the DOS. One of these missing peaks is always exactly at the frequency at which the sum is evaluated; here $x = \mathrm{Re}(x_0) \approx 9.8853$, again assuming $|\mathrm{Im}(x_0)| \ll \mathrm{Re}(x_0)$. Hence, using the smooth part of the DOS tends to overestimate the decay rate. Choosing various values of the refractive index n in the regime $x \leqslant 20$, we find numerically that this overestimation can be compensated by dividing the smooth part of the DOS by n [see Fig. 1(b)]. We cannot provide an analytical argument for this finding. Using the such modified smooth part of the DOS we approximate Eq. (34) by

$$\gamma = \gamma_0 + \frac{(n^2-1)\pi\,\mathrm{Re}(x_0)^3\sigma^2 W_m}{2nR^2}. \tag{48}$$

The replacement of the DOS by its smooth part can also be seen as an average over modes within a frequency window containing many modes. Thus, Eq. (48) is a result of an ensemble average and a frequency average.

For the special case of the Gaussian correlation function [Eq. (22)], condition (45) becomes

$$\frac{\Theta_c^2\,\mathrm{Re}(x_0)^2}{4}\left|\frac{m^2\Theta_c^2}{2} - 1\right| \ll 1. \tag{49}$$

The approximate result in Eq. (48) translates to

$$\gamma = \gamma_0 + \frac{(n^2-1)\sqrt{\pi}\mathrm{Re}(x_0)^3\sigma^2\Theta_c}{4nR^2}e^{-m^2\frac{\Theta_c^2}{4}}, \tag{50}$$

with $\vartheta(\Theta_c) \approx 1$ in the relevant regime of Θ_c. As the variance of the frequency splitting, $\gamma(\Theta_c)$ has a global maximum but now at $\Theta_c = \sqrt{2}/m$.

Formula (50) has an important consequence. Suppose we have two modes with similar frequency and azimuthal mode numbers $m_1 > m_2$. For the radial mode numbers it then must hold that $l_1 < l_2$. In the perfect disk, mode 1 usually has significantly lower losses than mode 2. In the opposite regime in which surface roughness dominates the losses, mode 1 has on average still lower losses because of the exponential in Eq. (50). However, the differences in the expected decay rates

can be negligible when the correlation angle Θ_c is sufficiently small. Fluctuation can then easily lead to a mode 2 with lower losses than mode 1.

VI. NUMERICAL RESULTS

In this section we verify our theory by a comparison to numerical results. We employ the boundary element method (BEM) [49] to compute the characteristics of the TM modes. If not stated otherwise we consider the mode pair $(m,l) = (16,1)$, the refractive index $n = 2$, the wavelength regime around $\lambda \approx 900$ nm, and the disk radius $R = 1.415\,\mu$m. For the surface roughness we assume a Gaussian correlation function (19). For all values of σ and Θ_c used in the following the condition for the validity of the theory in Eq. (43) is satisfied.

The surface roughness is implemented by expanding the deformation function into a Fourier series with complex coefficients A_q being random variables with first two moments as in Eqs. (20) and (21). To do so, we first pick the phase of each A_q randomly from a uniform distribution between zero and 2π. This ensures Eq. (20) and the Kronecker delta $\delta_{q,p}$ in Eq. (21). Second, we pick $|A_q|$ randomly from a uniform distribution in the interval $[0,\sigma\sqrt{3W_q}/R]$ where the upper border is chosen such that Eq. (21) is fulfilled for $q = p$. Another possibility (not shown) is to choose A_q to be independent circular symmetric Gaussian random variables with an appropriate variance. We find that both approaches give nearly the same results for the variance of the frequency splitting [Eq. (25)] and the expected decay rate [Eq. (34)]. However, fluctuations around these two mean values do depend on the choice of the probability distribution. In an extended version of the theory this would be incorporated by higher-order moments, such as $\langle A_q A_p A_r \rangle$, which are, however, not known for microdisks.

For a randomly picked realization of the cavity's boundary with $\sigma/R = 0.005$ and $\Theta_c = 0.07$, Fig. 4 shows the spatial mode structure of a mode pair. The values of the chosen roughness parameters correspond to a relatively large roughness standard deviation $\sigma = 7$ nm and a correlation length $L_c = 100$ nm. At first glance, the two modes look like conventional standing-wave modes with an equal amount of clockwise (CW) and counterclockwise (CCW) traveling waves. However, an angular momentum decomposition [50] reveals that for both modes the CCW intensity I_{CCW} is about 2.3 times larger than the CW intensity I_{CW}. This unbalanced contribution of CCW and CW traveling waves is quantified by the chirality [50]

$$\alpha = 1 - \frac{\min\left(I_{\mathrm{CCW}}, I_{\mathrm{CW}}\right)}{\max\left(I_{\mathrm{CCW}}, I_{\mathrm{CW}}\right)}. \tag{51}$$

Here, $\alpha \approx 0.57$ for both modes. The modes are therefore not standing waves ($\alpha = 0$) in contrast to the common wisdom (see, e.g., Refs. [6,8]) but partially copropagating traveling waves. This chirality is a generic feature of deformed or perturbed whispering-gallery cavities without any mirror-reflection symmetry [50–55]. The physical origin of this kind of chirality is asymmetric backscattering between CW and CCW traveling waves. It has to be emphasized that our statistical theory does not assume the backscattering to be symmetric.

The far-field pattern of the two modes is depicted in Fig. 4(c). A rather nonuniform emission distribution can be observed. This is in agreement with recent experiments [18].

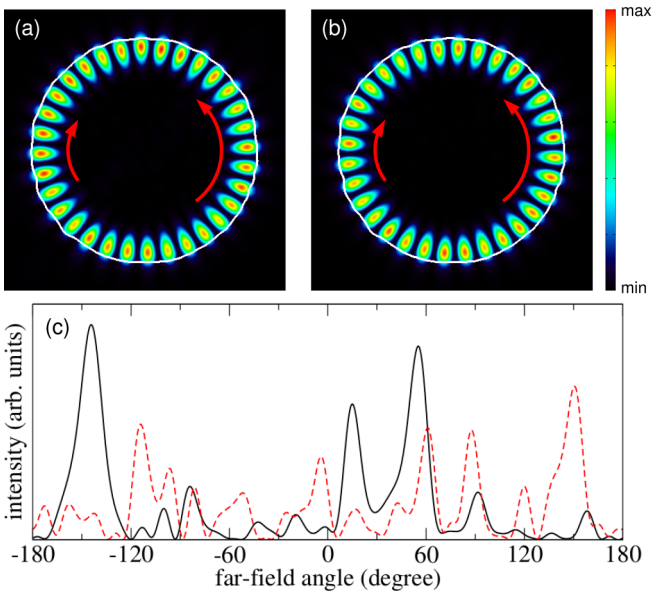

FIG. 4. Intensity $|\psi|^2$ of mode pair $(m,l) = (16,1)$ in a rough disk with $n = 2$, $\sigma/R = 0.005$, and $\Theta_c = 0.07$ (in radians) calculated numerically by the BEM. Dimensionless frequency (a) $x = 9.89497 - i0.00147$ and (b) $x = 9.89523 - i0.00054$. The arrows illustrate an unbalanced contribution of clockwise and counterclockwise traveling waves. (c) Far-field intensity pattern for the mode in (a) (solid curve) and (b) (dashed curve). The area below both curves is normalized to 1.

Figure 5(a) shows the (squared) frequency splittings of 60 realizations and the resulting variance as a function of σ/R. A very good agreement between theory and numerical calculations can be observed even for σ/R as large as 0.01 which translates for the chosen R to $\sigma = 14$ nm. There are considerable fluctuations around the expectation values. The

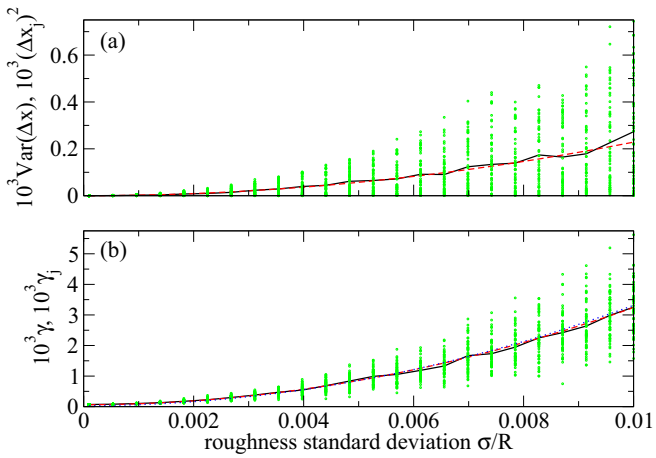

FIG. 5. (a) Variance of the (dimensionless) frequency splitting $\mathrm{Var}(\Delta x)$ and (b) expected (dimensionless) decay rate γ vs roughness standard deviation σ in units of R; $\Theta_c = 0.07$, $n = 2$, $(m,l) = (16,1)$. The green dots mark the individual results, $(\Delta x_j)^2$ and γ_j, of the BEM (60 realizations for each point on the σ axis). The solid black curves show the result of averaging. The dashed red curves are the perturbative results in Eqs. (26) and (36), respectively. The dotted blue curve in (b) is approximation (50). Note that the curves are partly on top of each other.

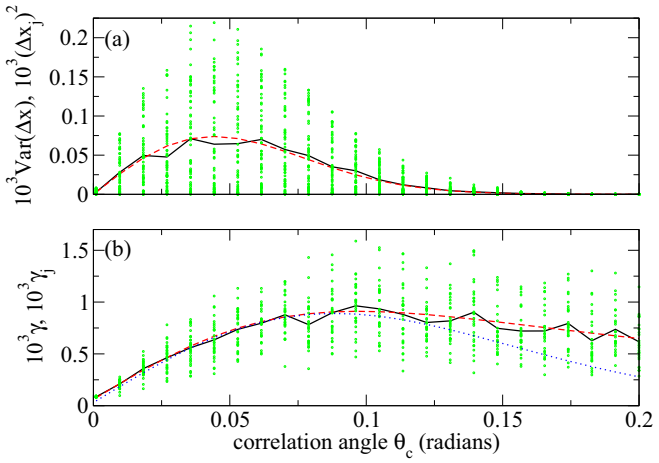

FIG. 6. (a) Variance of frequency splitting $\mathrm{Var}(\Delta x)$ and (b) expected decay rate γ vs correlation angle Θ_c; $\sigma/R = 0.005$, $n = 2$, $(m,l) = (16,1)$. The green dots mark the individual results of the BEM (60 realizations for each point on the Θ_c axis). The solid black curves show the result of averaging. The dashed red curves are the perturbative results in Eqs. (26) and (36), respectively. The dotted blue curve in (b) is approximation (50).

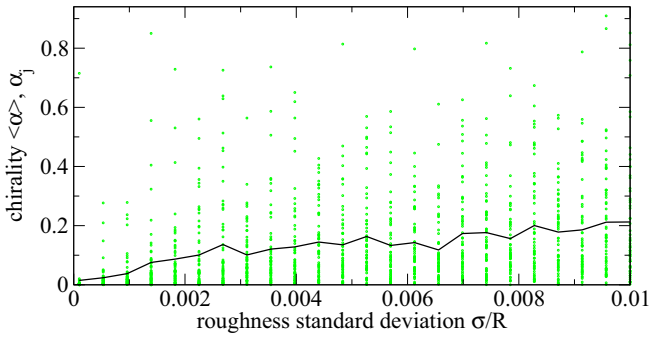

FIG. 7. Chirality of modes α [Eq. (51)] vs roughness standard deviation σ in units of R; $\Theta_c = 0.07$, $n = 2$, $(m,l) = (16,1)$. The green dots mark the individual results, α_j, of the BEM (60 realizations for each point on the σ axis). The solid black curve shows the result of averaging, $\langle\alpha\rangle$.

importance of such fluctuations was already discussed in the context of comparing frequency splittings of modes with different m in Ref. [10]. A statistical theory based solely on Eqs. (13)–(16) cannot predict the characteristics of individual realizations. It can, at best, give an estimation of its order of magnitude.

Figure 5(b) shows the decay rates of the same 60 realizations (averaged over the two modes of the mode pair) and the resulting averaged decay rate as a function of σ/R. Again, a very good agreement between theory and numerical calculations can be observed. In addition, Fig. 5(b) shows approximation (50), which can hardly be distinguished by eye from the full theoretical result.

The variation of the variance of the frequency splitting as a function of the correlation angle is shown in Fig. 6(a). The global maximum at $\Theta_c = 1/(\sqrt{2}m) \approx 0.044$ can be clearly seen. Figure 6(b) shows the expected decay rate as a function of Θ_c. This curve has a maximum around $\Theta_c \approx 0.096$ which is reasonably close to the prediction of the simplified theory (50): $\Theta_c = \sqrt{2}/m \approx 0.088$. In both cases the agreement between the theory and the full numerical calculations is very convincing. Note that even for small Θ_c the relative fluctuations are large (not shown). So, one cannot take advantage of self-averaging. Moreover, approximation (50) again agrees well with the full theoretical results. Deviations start to become visible around $\Theta_c \approx 1.25$ where condition (49) is no longer fulfilled.

Figure 7 shows the chirality α of the modes as a function of σ. Whereas the averaged chirality is well below $1/4$ for the considered regime of σ, the fluctuations can lead to significant chirality close to 1 even for small σ. We do not have a statistical theory for the chirality induced by the surface roughness since the resulting perturbation series contains other terms than in Eqs. (20) and (21). The same is true for properties related to the far-field pattern.

VII. COMPARISON TO LITERATURE

Finally, we compare the results of our theory to measured data from the literature. Unfortunately, none of the experiments had performed an ensemble average, for which it would be necessary to measure many independently fabricated cavities under the same conditions.

The authors of Ref. [8] measured the quality factor Q and the wavelength splitting $\Delta\lambda$ for two silicon microdisk cavities of different size. Their study included a reconstruction of the correlation function based on a single realization assuming ergodicity. They demonstrated a clear Gaussian behavior as in Eq. (18) with $\sigma = 2.8$ nm and $L_c = 40$ nm. For the first disk with radius $R = 2.5\,\mu$m they found for the TM mode (23,1) the values $Q = 4.7 \times 10^5$ and $\Delta\lambda = 93$ pm. For the second disk with $R = 4.5\,\mu$m they measured for the TM mode (44,1) the values $Q = 5.2 \times 10^5$ and $\Delta\lambda = 37$ pm. For comparison we estimate from the spectrum in the inset of Fig. 2(a) in Ref. [8] an effective index $n = 2.75$ and approximate Q by $\mathrm{Re}(x_0)/(2\gamma)$. Condition (43) is fulfilled. For the smaller disk with $R = 2.5\,\mu$m we get from Eq. (36) the quality factor $Q \approx 1.8 \times 10^5$ and from Eq. (26) the wavelength splitting $\Delta\lambda = 221$ pm. This gives a reasonable agreement, having in mind that we compare expectation values to a single realization. For the larger disk ($R = 4.5\,\mu$m) we get $Q \approx 3.4 \times 10^5$ and $\Delta\lambda = 90$ pm, again in similar agreement with the experiment.

Next, we compare our theory to experimental data obtained by the same group also for silicon microdisks but with reduced surface roughness [7]. Unfortunately, the roughness parameters have not been independently determined but were estimated by fitting numerical results to experimentally measured doublet splitting parameter $Q_\beta = \lambda/\Delta\lambda$ and quality factors. Since a simultaneous fit was not successful the authors in Ref. [7] proposed the existence of another relevant decay channel, namely, surface state absorption. In contrast, our (simplified) theory permits such a fit with reasonable parameters without extra decay channel (see Fig. 8). We compute the doublet splitting parameter by $Q_\beta = \mathrm{Re}(x_0)/\sqrt{\mathrm{Var}(\Delta x)}$ and the quality factor again by $Q = \mathrm{Re}(x_0)/(2\gamma)$. We choose the same effective index n mentioned above and take the wavelength λ to be $1.455\,\mu$m located at the center of the wavelength range $1.41-1.5\,\mu$m studied in Ref. [7]. The decay

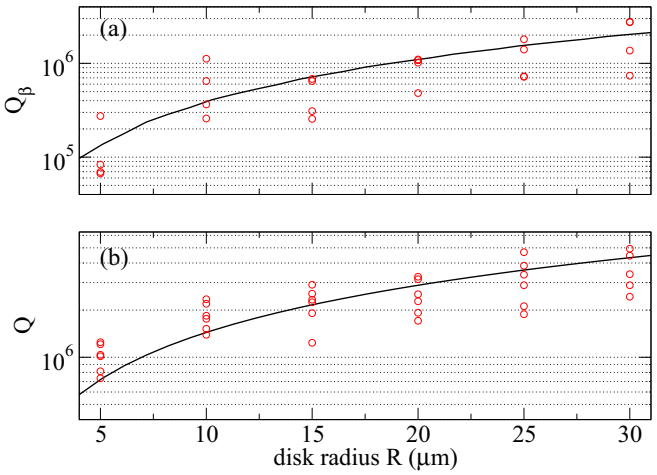

FIG. 8. (a) Doublet splitting parameter Q_β computed from Eq. (26) and (b) Q factor computed from Eq. (50) vs radius R (solid curves) in a semilogarithmic scale; $\sigma = 1.75$ nm, $L_c = 180$ nm, $n = 2.75$, $\lambda = 1.455\,\mu$m, and $m = 2\pi nR/\lambda$. Open circles represent the experimental data extracted from Ref. [7].

rate for the perfect disk, γ_0, can be safely ignored for $R \geqslant 5\,\mu$m. The azimuthal mode index m is determined with the asymptotic relation $m = n\mathrm{Re}(x_0) = 2\pi nR/\lambda$ [30]. Finally, we adjust the roughness parameters to $\sigma = 1.75$ nm and $L_c = 180$ nm, which fulfills conditions (43) and (49). A very satisfactory agreement between experimental data and our theory can be observed for both Q_β and Q simultaneously. Note that the experimental data do not involve an ensemble average.

A direct comparison to other theoretical works using the volume element method is hindered by the usage of various approximations (for instance $\Theta_c \ll 1$, $\mathrm{Re}(x_0) \approx m/n$ for large m, correlation functions with $\mathcal{W}'(0) = 0$, and symmetric backscattering between CW and CCW traveling waves) which are sometimes not mentioned [7,8,17,39,40]. Often, results are given only implicitly (e.g., Ref. [39]) and prefactors are unclear (e.g., Ref. [17]). In limiting cases our formulas are sometimes similar to the ones found by the volume element method but differ by a prefactor of order 1. For example, Eq. (26) agrees with the one in Ref. [8] apart from a factor of $\pi^2/16 \approx 0.62$.

VIII. CONCLUSION

We have introduced a statistical theory for sidewall roughness of microdisk cavities in the effective index approximation for the TM polarized electromagnetic modes. The approach is based on a recently developed perturbation theory for microdisks with weak boundary deformation. Explicit formulas for the variance of the frequency splitting and the expectation value of the decay rates are derived and explained. For a Gaussian correlation function it is shown that both quantities show a global maximum as a function of the correlation angle. This provides a strategy to reduce the effects of surface roughness by increasing the correlation angle.

A comparison to full numerical results based on the boundary element method shows excellent agreement even for rather strong surface roughness. The numerical results also reveal the appearance of rather strong fluctuations around the expectation values and the presence of chirality of the modes induced by the surface roughness. We have applied our theory to experimental data from the literature and observe reasonable agreement. We have taken advantage of the fact that our theory is not restricted to small correlation angles. This allows us to demonstrate that no additional decay channel is needed to explain the experimental data of Ref. [7]. We believe that our work will help to understand and improve the properties of optical microcavities.

ACKNOWLEDGMENTS

The authors thank H. Cao for interesting discussions, and O. Painter and M. Borselli for the permission to use their experimental data. This work was supported by the DFG (Project No. WI1986/7-1).

[1] K. J. Vahala, Nature (London) **424**, 839 (2003).
[2] F. Vollmer and L. Yang, Nanophotonics **1**, 267 (2012).
[3] L. He, Ş. K. Özdemir, and L. Yang, Laser Photonics Rev. **7**, 60 (2013).
[4] H. Cao and J. Wiersig, Rev. Mod. Phys. **87**, 61 (2015).
[5] M. L. Gorodetsky, A. A. Savchenkov, and V. S. Ilchenko, Opt. Lett. **21**, 453 (1996).
[6] M. L. Gorodetsky, A. D. Pryamikov, and V. S. Ilchenko, J. Opt. Soc. Am. B **17**, 1051 (2000).
[7] M. Borselli, J. Johnson, and O. Painter, Opt. Express **13**, 1515 (2005).
[8] M. Borselli, K. Srinivasan, P. E. Barclay, and P. Painter, Appl. Phys. Lett. **85**, 3693 (2004).
[9] X. Zhang, H. S. Choi, and A. M. Armani, Appl. Phys. Lett. **96**, 153304 (2010).
[10] Q. Li, A. A. Eftehkar, Z. Xia, and A. Adibi, Opt. Lett. **37**, 1586 (2012).
[11] S. L. McCall, A. F. J. Levi, R. E. Slusher, S. J. Pearton, and R. A. Logan, Appl. Phys. Lett. **60**, 289 (1992).
[12] C. P. Michael, K. Srinivasan, T. J. Johnson, O. Painter, K. H. Lee, K. Hennessy, H. Kim, and E. Hu, Appl. Phys. Lett. **90**, 051108 (2007).
[13] M. Witzany, R. Roßbach, W.-M. Schulz, M. Jetter, P. Michler, T.-L. Liu, E. Hu, J. Wiersig, and F. Jahnke, Phys. Rev. B **83**, 205305 (2011).
[14] B. J. Li and P.-L. Liu, IEEE J. Quantum Electron. **33**, 791 (1997).
[15] A. I. Rahachou and I. V. Zozoulenko, J. Appl. Phys. **94**, 7929 (2003).
[16] C. Sui, Q. Wang, S. Xiao, and P. Li, Opt. Photonics J. **3**, 288 (2013).
[17] J. E. Heebner, T. C. Bond, and J. S. Kallman, Opt. Express **15**, 4452 (2007).
[18] S. F. Liew, B. Redding, L. Ge, G. S. Solomon, and H. Cao, Appl. Phys. Lett. **104**, 231108 (2014).
[19] S. F. Liew, L. Ge, B. Redding, G. S. Solomon, and H. Cao, Phys. Rev. A **91**, 043828 (2015).
[20] S. F. Liew, L. Ge, B. Redding, G. S. Solomon, and H. Cao, Appl. Phys. Lett. **108**, 051105 (2016).

[21] K. M. Frahm and D. L. Shepelyansky, Phys. Rev. Lett. **78**, 1440 (1997).
[22] L. Sirko, S. Bauch, Y. Hlushchuck, P. M. Koch, R. Blümel, M. Barth, U. Kuhl, and H.-J. Stöckmann, Phys. Lett. A **266**, 331 (2000).
[23] O. A. Starykh, P. R. J. Jacquod, E. E. Narimanov, and A. D. Stone, Phys. Rev. E **62**, 2078 (2000).
[24] V. A. Podolskiy, E. Narimanov, W. Fang, and H. Cao, Proc. Natl. Acad. Sci. USA **101**, 10498 (2004).
[25] W. Fang, H. Cao, V. Podolskiy, and E. Narimanov, Opt. Express **13**, 5641 (2005).
[26] J. U. Nöckel and A. D. Stone, Nature (London) **385**, 45 (1997).
[27] J. Wiersig and M. Hentschel, Phys. Rev. Lett. **100**, 033901 (2008).
[28] X.-F. Jiang, Y.-F. Xiao, C.-L. Zou, L. He, C.-H. Dong, B.-B. Li, Y. Li, F.-W. Sun, L. Yang, and Q. Gong, Adv. Mater. **24**, OP260 (2012).
[29] S. Sunada, S. Shinohara, T. Fukushima, and T. Harayama, Phys. Rev. Lett. **116**, 203903 (2016).
[30] R. Dubertrand, E. Bogomolny, N. Djellali, M. Lebental, and C. Schmit, Phys. Rev. A **77**, 013804 (2008).
[31] L. Ge, Q. H. Song, B. Redding, and H. Cao, Phys. Rev. A **87**, 023833 (2013).
[32] J. Wiersig, Phys. Rev. A **85**, 063838 (2012).
[33] L. Ge, Q. Song, B. Redding, A. Eberspächer, J. Wiersig, and H. Cao, Phys. Rev. A **88**, 043801 (2013).
[34] B. Redding, L. Ge, Q. H. Song, G. S. Solomon, and H. Cao, Phys. Rev. Lett. **112**, 163902 (2014).
[35] M. Kraft and J. Wiersig, Phys. Rev. A **89**, 023819 (2014).
[36] M. Kraft and J. Wiersig, Phys. Rev. A **94**, 013851 (2016).
[37] J. Kullig and J. Wiersig, Phys. Rev. E **94**, 022202 (2016).
[38] J. Kullig and J. Wiersig, Phys. Rev. A **94**, 043850 (2016).
[39] E. M. Ganapolskii, Z. E. Eremenko, and Y. V. Tarasov, Phys. Rev. E **79**, 041136 (2009).
[40] E. M. Ganapolskii, Y. V. Tarasov, and L. D. Shostenko, Phys. Rev. E **84**, 026209 (2011).
[41] J. D. Jackson, *Classical Electrodynamics* (John Wiley and Sons, New York, 1962).
[42] F. M. Izrailev and N. M. Makarov, in *Structured Surfaces as Optical Metamaterials*, edited by A. A. Maraduin (Cambridge University Press, Cambridge, U.K., 2011), p. 287.
[43] Q. J. Wang, C. Yan, N. Yu, J. Unterhinninghofen, J. Wiersig, C. Pflügl, L. Diehl, T. Edamura, M. Yamanishi, H. Kan, and F. Capasso, Proc. Natl. Acad. Sci. USA **107**, 22407 (2010).
[44] N. L. Aung, L. Ge, O. Malik, H. E. Türeci, and C. F. Gmachl, Appl. Phys. Lett. **107**, 151106 (2015).
[45] C. A. Bader, F. Zeuner, M. H. W. Bader, T. Zentgraf, and C. Meier, J. Appl. Phys. **118**, 213105 (2015).
[46] A. M. Yaglom, *An Introduction to the Theory of Stationary Random Functions* (Dover, Mineola, NY, 2004).
[47] F. W. J. Olver, D. W. Lozier, R. F. Boisvert, and C. W. Clark, *NIST Handbook of Mathematical Functions* (Cambridge University Press, New York, 2010).
[48] E. Bogomolny, R. Dubertrand, and C. Schmit, Phys. Rev. E **78**, 056202 (2008).
[49] J. Wiersig, J. Opt. A **5**, 53 (2003).
[50] J. Wiersig, S. W. Kim, and M. Hentschel, Phys. Rev. A **78**, 053809 (2008).
[51] J. Wiersig, A. Eberspächer, J.-B. Shim, J.-W. Ryu, S. Shinohara, M. Hentschel, and H. Schomerus, Phys. Rev. A **84**, 023845 (2011).
[52] J. Wiersig, Phys. Rev. A **89**, 012119 (2014).
[53] R. Sarma, L. Ge, J. Wiersig, and H. Cao, Phys. Rev. Lett. **114**, 053903 (2015).
[54] J. Kullig and J. Wiersig, New J. Phys. **18**, 015005 (2016).
[55] B. Peng, Ş. K. Özdemir, M. Liertzer, W. Chen, J. Kramer, H. Yilmaz, J. Wiersig, S. Rotter, and L. Yang, Proc. Natl. Acad. Sci. USA **113**, 6845 (2016).